Design of a Radar Signature Measurement Model of an Unmanned Aerial Vehicle with Low Radar Signature

Harmen van der Ven[1], David Escot Bocanegra[2], Jesús Álvarez González[2], Mehmet Erim İnal[3], Askin Altinoklu[3], Alper Kürşat Öztürk[4], Ulrich Jakobus[5], Andrey Osipov[6], Øystein Lie-Svendsen[7], Frank Weinmann[8], Åsa Andersson[9], Henrik Edefur[9], Jan-Ove Hall[9], David Poyatos Martínez[10], Tolga Çiftçi[11], and Şükrü Tarık Kostak[11]

[1]Royal National Aerospace Center (NLR)
A. Fokkerweg 2, Amsterdam, The Netherlands
harmen.van.der.ven@nlr.nl

[2]Airbus Defence and Space
Calle Aviocar, 2 28906 Getafe, Spain
david.escot@airbus.com, jesus.g.alvarez@airbus.com

[3]Aselsan Inc.
Konya Yolu 8.km Ogulbey Mah, 3051. Sokak No:3, 06830 Ankara, Turkiye
inal@aselsan.com.tr, aaltinoklu@aselsan.com.tr

[4]RAPIDEM LLC
Bilkent CyberPark B-222, Cankaya, Ankara, Turkiye
alperkozturk@gmail.com

[5]Altair Engineering GmbH
Calwer Str. 7, D-71034 Böblingen, Germany
jakobus@altair.com

[6]German Aerospace Center (DLR)
DLR Microwaves and Radar Institute, Muenchener Strasse 20, 82234 Wessling, Germany
andrey.osipov@dlr.de

[7]Norwegian Defence Research Establishment (FFI)
P.O. Box 25, NO-2027 Kjeller, Norway
oystein.lie-svendsen@ffi.no

[8]Fraunhofer Institute for High Frequency Physics and Radar Techniques FHR
Fraunhoferstraße 20, 53343 Wachtberg, Germany
frank.weinmann@fhr.fraunhofer.de

[9]Swedish Defence Research Agency (FOI)
SE-164 90 Stockholm, Sweden
asa.andersson@foi.se, henrik.edefur@foi.se, jan-ove.hall@foi.se

[10]National Institute of Aerospace Technology (INTA)
Ctra. de Ajalvir, Km. 4,5, 28850 Torrejón de Ardoz, Madrid, Spain
poyatosmd@inta.es

[11]Turkish Aerospace
Fethiye Mahallesi, Havacilik Bulvari No:17, Kahramankazan Ankara, Turkiye
tolga.ciftci@tai.com.tr, sukrutarik.kostak@tai.com.tr

Submitted On: January 21, 2024
Accepted On: August 7, 2024

https://doi.org/10.13052/2024.ACES.J.390602

Abstract – Existing databases of RCS benchmarks lack a complex, low-observable target. This paper describes the design of such a complex and low-observable measurement model. Starting point of the design is the so-called Muldicon model, developed by the NATO/STO/AVT panel. Hot spots of the original model are identified and treated with radar-absorbing materials. Simulations on the treated model demonstrate that the model is indeed low observable. The effect of the manufacturing process of 3D-printing and separable parts is assessed experimentally on a cone-sphere; the effect is found to be negligible. These results give confidence that the model, when built, satisfies the requirements of being complex and low observable; and that artefacts of the manufacturing process will not impair its signature.

Index Terms – Low observable, measurement model, radar signature.

I. INTRODUCTION

With the ever-increasing use of computational electromagnetics, there is a constant need to validate the computational tools with measurement data. The pioneering work of Woo et al. [1] presented a first set of canonical test cases which still serve as benchmarks for the validation of computational tools [2]. More databases for validation followed [3][4]. The publicly available Austin RCS benchmark suite [4] is the most recent; it contains canonical geometries, but also a generic military aircraft. Moreover, the suite not only contains perfectly electrically conducting (PEC) bodies, but also (fully homogeneous) dielectric bodies [5].

Military aircraft generally are designed to have low radar signature by shaping and the application of radar-absorbing materials. This type of target is missing in the above databases: complex targets with doubly curved surfaces, sharp edges, concealed inlet, with radar-absorbing materials. The resulting low signature (typically one or two orders of magnitude less than the size would suggest) poses challenges to computational tools, since the correct modelling of small details becomes important.

This paper presents the design of a low-observable unmanned aerial combat vehicle (UCAV) measurement model. In future, it could serve as a standard problem for validation (in the formulation of the IEEE standard on validation [6]). Starting point of the design is the so-called Muldicon model developed by the NATO/STO/AVT panel [7], as a paper exercise for multidisciplinary design (aerodynamic and structural properties were considered). Figure 1 presents both the outer mold of the aircraft and the inlet and outlet. The aircraft has certain features which may lead to a low signature, such as a concealed air intake. Nonetheless, the aircraft shape has not been driven, nor comprised, by its radar signature, so its signature has not been optimized. Changing the outer mold will require a new design loop to assure the aerodynamic characteristics of the aircraft. Its signature can only be reduced by the application of radar absorbing materials (RAM).

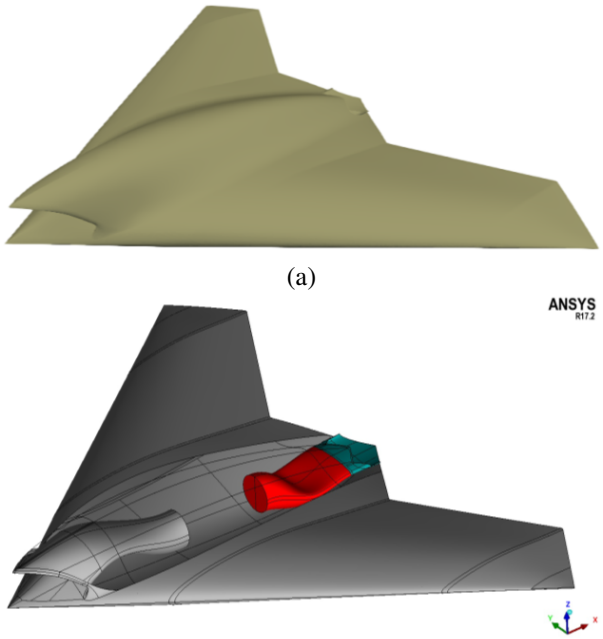

(a)

(b)

Fig. 1. Geometry of the unmanned aerial vehicle Muldicon [7]: (a) outer mold and (b) inlet and outlet.

This paper will address some of the topics in the design process. The design and manufacturing of the measurement model has been the task of the NATO/STO/SET-252 Task Group [8]. It was a five-year effort of the authors of the present paper. Obviously, there is not enough space to incorporate all details of the design process.

The structure of this paper is as follows. In Section II the design requirements and an overall design of the model is presented. Section III contains a hot spot analysis which will be used to reduce the nose-on signature. Parts of the model will be 3D printed; the required accuracy of the printing process is assessed experimentally in Section IV. Section V contains a computational assessment of the low observability characteristics of the measurement model. Finally, Section VI draws the conclusions of the study.

II. OVERALL DESIGN OF THE MEASUREMENT MODEL

As stated in the introduction the overall objective is to design a low-observable, complex, radar signature

measurement model. The requirement on geometrical complexity of the model is satisfied for the Muldicon. Modeling complexity will be satisfied by the application of radar-absorbing material which shall reduce the RCS by at least 10 dB in the nose section. The model will be measured at different sites, so must be transportable.

The measurement model will be measured at a center frequency of 10 GHz. RAM is applied to certain parts of the aircraft to reduce the radar signature. The RAM can be narrowband RAM since no broadband measurements are foreseen.

The span of the model will be 3 meters. The size is a compromise. On the one hand, the model should be sufficiently large to correspond to the objects of practical interest (UCAV, drones), and the field scattered by the model should be sufficiently strong to be registered by the receiving system of an RCS measurement facility with enough signal-to-noise ratio to ensure high accuracy of the results and good dynamic range. On the other hand, its electrical size should permit numerical evaluation of RCS with commercial EM solvers and fit into the quiet zone of a typical compact test range RCS measurement facility. The weight of the model (which is directly related to its size) should be acceptable for the supporting and positioning structures of the measurement facilities and allow uncomplicated transportation between measurement sites. Moreover, RCS measurement of a three meters object can also be performed on outdoor test ranges which will provide further benchmarking activities.

Because of the transportation requirement, the model consists of three separable parts: two wings and a midsection. The midsection is 3D printed because of the level of geometrically detail required for the inlet, outlet, turntable insert, and the spars connecting to the wings. This level of detail can also be obtained through milling, but at a higher cost. Since the wings are large smooth surfaces, they are milled from foam. A nickel paint is applied to the full aircraft to ensure a PEC surface.

This design prompts the following research questions: (1) what are the appropriate locations for the RAM patches to reduce the signature and (2) what are the resolution requirements for the 3D-printing process?

III. HOT SPOT ANALYSIS

To ascertain the radar signature of the untreated, fully PEC, model, the monostatic RCS for both vertical and horizontal polarization is computed. Computations are performed using RAPID [9], with the combined field integral equation (CFIE) formulation and multilevel fast-multipole (MLFMM) acceleration. Results are shown in Fig. 2.

The HH polarization shows two spiky maxima at $\phi = 53^\circ$ and $\phi = 150^\circ$. These azimuthal angles are the

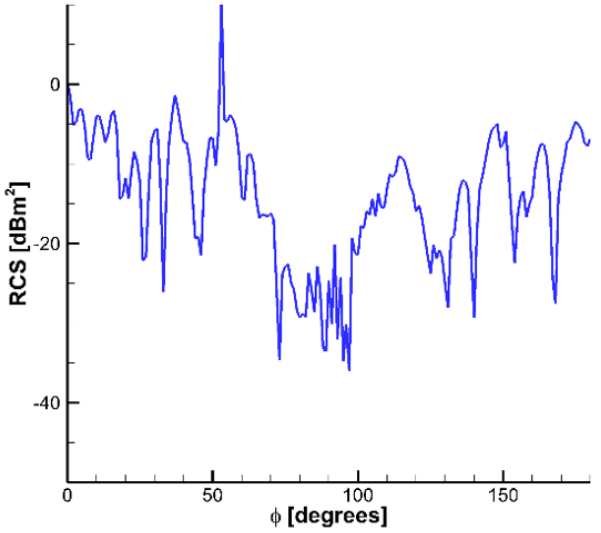

(a)

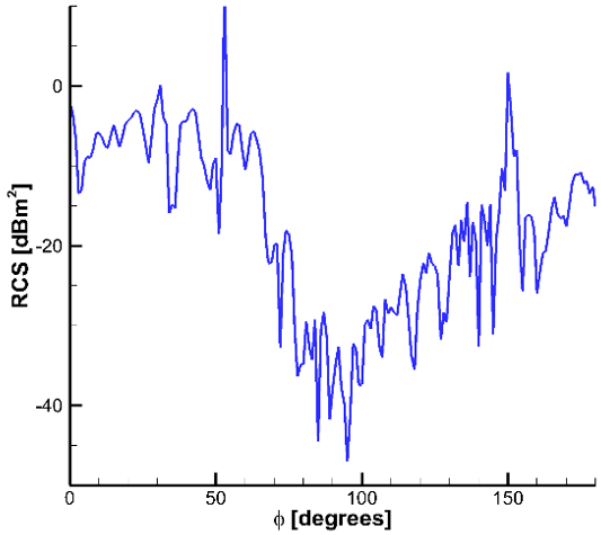

(b)

Fig. 2. RCS at 10 GHz of the untreated Muldicon as a function of azimuth angle ϕ in the zero elevation plane, where $\phi = 0^\circ$ corresponds to nose-on illumination: (a) VV polarization and (b) HH polarization.

starboard leading edge and the trailing edges of the delta wing. It is also obvious from the RCS characteristics for both polarizations that a significant RCS increase accumulates around the nose sector. As the future measurements will be performed for frontal aspects, it is worthy to investigate the RCS contributors of the illumination angles $\phi = 0^\circ$ and $\phi = 53^\circ$.

In order to calculate the hot spots on the 3D surface model for a given illumination angle, the currents induced on the surface of the mesh model are post-processed through a specific method [10]: the RCS contribution of the induced currents within a certain

neighborhood of each point on the surface of the mesh model is calculated and this value is assigned to the associated point. This yields a color map of RCS contribution surfaces of the mesh model, namely, the hot spot areas on the surface.

Results are shown in Fig. 3. It is clear that the leading edge of the wing and the inlet are the dominant RCS contributors for $\phi = 53°$. The dominant RCS contributor for nose on is the inlet. These two regions will be treated with a commercially available narrowband magnetic absorber which is effective at 10 GHz.

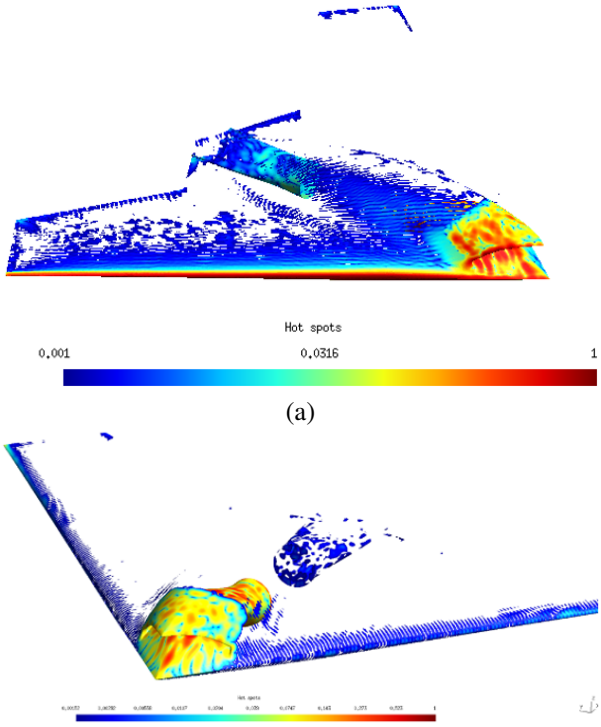

(a)

(b)

Fig. 3. Hot spot areas (in red) for horizontal polarization: (a) hot spot analysis for $\phi = 53°$ and (b) hot spot analysis for $\phi = 0°$ (nose on).

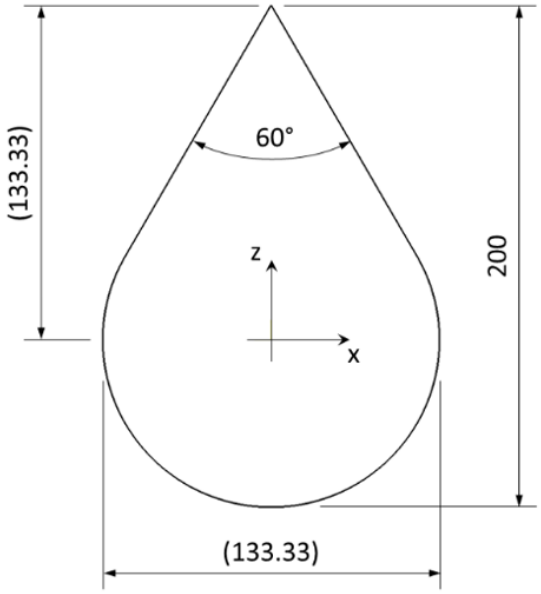

Fig. 4. Cone-sphere dimensions (in mm).

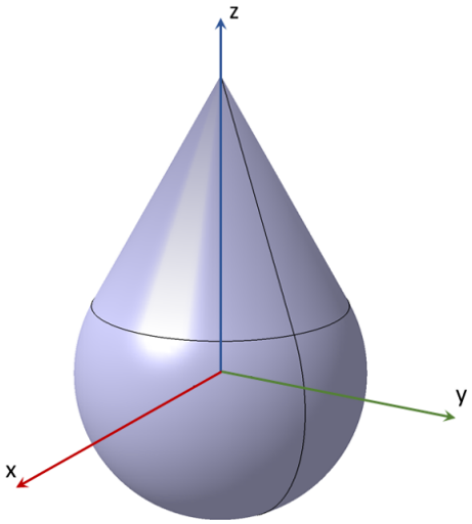

Fig. 5. Cone-sphere coordinate system.

IV. 3D PRINTING

The midsection of the Muldicon will be 3D printed. This process will not result in a smooth surface as the filament is applied in layers. In order to assess the effect of the surface roughness on the radar signature, four different 3D cone-spheres are fabricated with different finishes and conductivity, in addition to an aluminum cone-sphere as reference. The dimensions are defined in Fig. 4 and the coordinate system is shown in Fig. 5.

The objective of this study is to assess the effect of geometrical impurities on the radar signature. It is expected that if the print resolution is high enough in relation with the radar frequency, the surface can be considered to be smooth; and hence can be modeled as a smooth surface in the validation simulations. Therefore, radar signatures of the impure rough geometries will be compared directly with the signature of a smooth cone-sphere and no effort is made to quantify the surface roughness. The interested reader is referred to [11, 12], which measure and assess the surface roughness due to 3D-printing. The current study is performed at the same frequency which will be used for the Muldicon measurements. Since the cone-sphere has a low signature in the cone section, it is reasonable to expect that the results can be extrapolated to the Muldicon.

A. Model definition

A conventional fused filament fabrication (FFF) [13] 3D-printer is used to manufacture the cones at FOI. A thermoplastic material, in the form of a continuous filament, is fed from a large spool through a moving heated extruder head and deposited layer by layer on a growing object. The head is moved in two dimensions under computer control depositing one layer at a time to define the printed shape. The print head is then moved vertically by a small amount to begin the next layer. Increased layer thickness and/or larger nozzle diameter reduces the time it takes to print the object, but it also increases the surface roughness, potentially affecting the scattering of electromagnetic waves, or increasing the manual work needed afterwards. Hence, print time and surface roughness tolerance must be balanced.

The cone-spheres are printed in two sections (see Fig. 6) to avoid print support. The sections have a small central hole where a peg is placed to align the cone and sphere section during assembly. This peg also increases the bond between the parts when glued together.

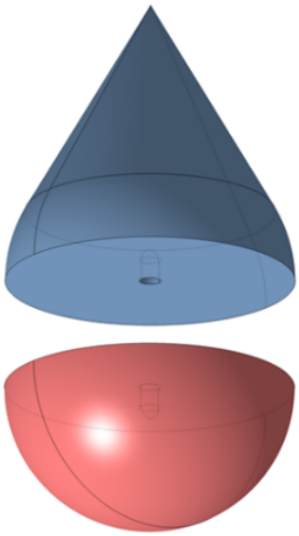

Fig. 6. Cone-sphere print sections.

To give the cone-spheres a PEC surface, the models are spray-painted with several layers of copper-based paint (Kontakt Chemie EMI 35 [14]). The surfaces are cleaned and degreased before painting to maintain the surface imperfections resulting from the print process.

The five models are:

- Cone-sphere A: Nozzle size 0.4 mm, layer height 0.2 mm. Standard PLA-filament (PrimaCreator EasyPrint PLA). Pieces glued together and then PEC-coated, which gives a "seamless" cone-sphere.
- Cone-sphere B: Nozzle size 0.8 mm, layer height 0.4 mm. Standard PLA-filament (PrimaCreator EasyPrint PLA). Pieces glued together and then PEC-coated, which gives a "seamless" cone-sphere.
- Cone-sphere C: Nozzle size 0.4 mm, layer height 0.2 mm. Standard PLA-filament (PrimaCreator EasyPrint PLA). Pieces PEC-coated and then glued together to simulate wing-fuselage joint.
- Cone-sphere D: Nozzle size 0.4 mm, layer height 0.2 mm. Electric conducting PETG-filament [15] (resistivity 106-109 ohm-cm). Pieces joined with a central metal screw.
- Cone-sphere E: fully metallic with smooth surface.

Cone-spheres A and B were designed to investigate the effect of surface roughness due to layer height but also other minor print artifacts. Figures 7 and 8 show a close-up of the surfaces after coating with electric conducting copper paint. Cone-sphere C was designed to investigate if there are any effect on the RCS due to a non-perfect joint between two PEC surfaces, similar to the joint between the wing and central fuselage sections of the Muldicon. To simulate this kind of joint, the spherical and cone section of the cone-sphere were

Fig. 7. Cone-sphere A.

Fig. 8. Cone-sphere B.

coated with copper paint separately (including the joining surface) and glued together afterwards. The purpose of cone-sphere D is to investigate if PETG could be a viable alternative to PLA coated with conductive paint.

B. Measurements

The measurements were carried out in the INTA Compact Antenna Test Range (CATR) at 10 GHz, the Muldicon frequency, and for cone-to-sphere aspects (polar angle $0^\circ < \theta < 180^o$).

C. Simulation

With the aim of comparing in a better way the measurements made, a smooth PEC cone-sphere is also simulated with Methods of Moments CFIE using FEKO [16].

D. Comparison and evaluation

Results will be shown for vertical ($\theta\theta$) polarization. The results for horizontal polarization are similar. Figure 9 (a) compares the measurement and simulation for the smooth PEC cone-sphere. The agreement is very good, except near the tip ($\theta = 0^o$). These discrepancies could be explained by the fact that, in the tip, the reflected field is very weak and the signal-to-noise ratio at the receiver is low, limiting the accuracy of the measurement results. Nevertheless, the overall agreement provides confidence in the measurement setup.

Measurements at 10 GHz for vertical polarization are shown in Fig. 9 (b). The objective is to see if different manufacturing techniques have significant effects and if the different specimens have comparable signature to the perfect metallic specimen E.

Negligible differences between specimen A (nozzle size 0.4 mm) and specimen B (nozzle size 0.8 mm) can be seen, except for the tip ($\theta = 0^o$). It can be concluded that the reduction in nozzle size is only relevant for very small and sharp geometrical details. It is not expected to find any effect on the fabricated Muldicon due to the nozzle size.

Studying specimen B (nozzle size 0.8 mm, layer height 0.4 mm) in detail and comparing with the metallic specimen E, again only the tip of the cone-sphere displays higher RCS. Hence the layer height will not cause any relevant effect on the final fabricated Muldicon.

Also, there are negligible differences between specimen A (pieces glued together and then PEC-coated) and specimen C (pieces PEC-coated and then glued together). PEC paint seems to work fine in both cases. It can be concluded that no effect on the Muldicon RCS is expected due to the joint between the wing and central fuselage sections when fabricated separately and joined afterwards as planned.

Finally, specimen D (PETG material) shows a lower RCS due to the low conductivity of the raw material. Thus, this material is not an alternative for fabrication purposes.

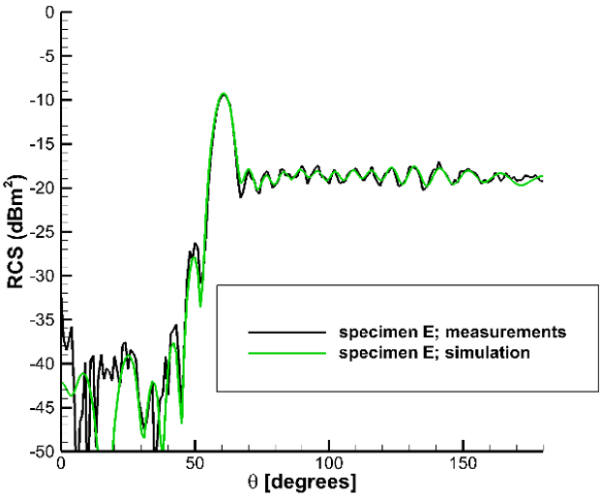

(a)

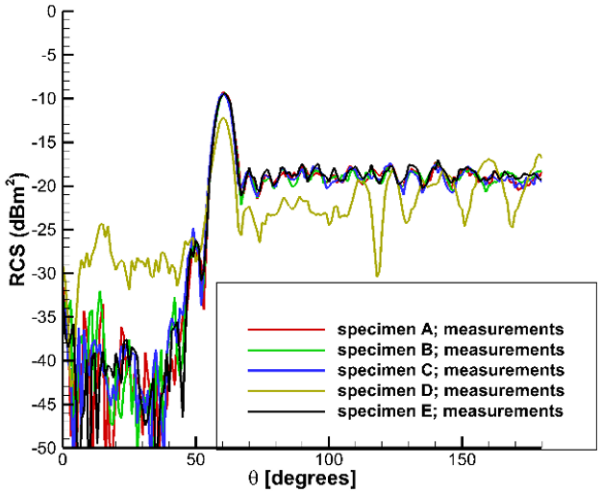

(b)

Fig. 9. Comparison of simulation and measurement results on the cone-sphere at 10 GHz for vertical polarization: (a) results comparison of measurement and simulation for the PEC cone-sphere and (b) comparison of the measurements.

V. SIMULATION OF TREATED MULDICON

Figure 10 shows a closeup of the model, depicting the areas where RAM is applied. Note that the leading edge of the right wing is not treated. For the physical model Laird SF-10 RAM [17] will be used. The tiles have a thickness of 1.35 mm and material properties: $\varepsilon_r = 13.29\text{-}0.25$ j and $\mu_r = 1.64\text{-}1.2$ j. There is no tapering of the tiles at their edges.

Two common meshes have been generated (but not used by all authors). Mesh A: a single layer mesh with a mesh width of $\lambda_0/10$ (where λ_0 is the wave length in vac-

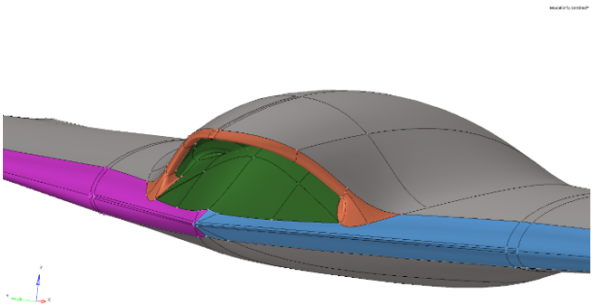

Fig. 10. Computational model of the treated Muldicon. The green and blue areas are treated with a narrowband RAM. The orange, purple and grey areas are PEC.

uum) when impedance boundary conditions (IBC) are used. Mesh B: a standard double layer mesh with a mesh width of $\lambda_0/10$ when the RAM is modeled as a dielectric. A brief overview of the simulation settings is given in Table 1, all (but one) using integral equation solvers with MLFMM acceleration. The impedance η in the IBC is computed as $\eta = j\sqrt{\frac{\mu_r}{\varepsilon_r}}\tan(k_0 d\sqrt{(\varepsilon_r \mu_r)})$, where ε_r, μ_r, d, and k_0 are the relative permittivity of the dielectric, its relative permeability, the thickness of the dielectric layer, and the free-space wave number. The motivation for using different meshes is, on the one hand, that the mesh structure is dictated by the method (IBC does not require a double layer; the finite-element boundary integral method requires a volume mesh in the RAM). On the other hand, the experience from different partners with their method of choice leads to different meshing strategies which produce the best results for the method considered.

The simulation results at elevation zero are shown in Fig. 11. It is clear from the difference between the left and right wing aspects that the treatment of the leading

Table 1: Overview of simulation settings

Partner	Method	Mesh
Airbus	in-house tool; both IBC and full dielectric [18]	A & B
Altair	FEKO [16]; IBC	A
Aselsan	in-house tool [9]; both IBC and full dielectric; JMCFIE formulation of [19]	own
FHR	in-house tool [20]: coupled boundary integral with finite element for dielectric	own
FOI	FEKO; IBC	A
INTA	FEKO; IBC	own
NLR	in-house tool [21]: full dielectric (Müller formulation)	B

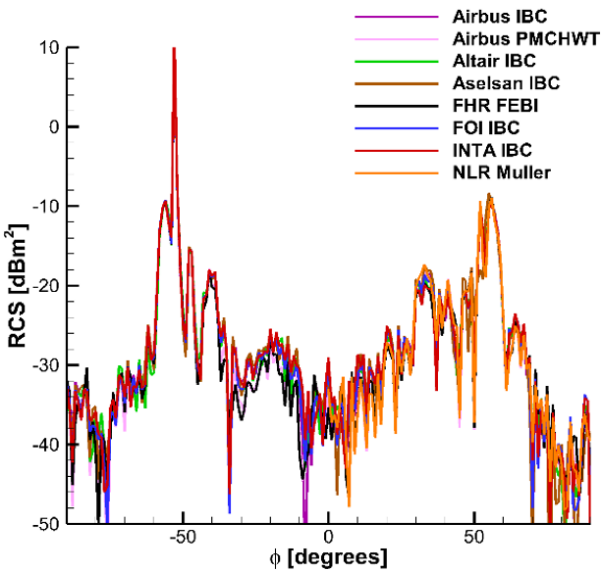

(a)

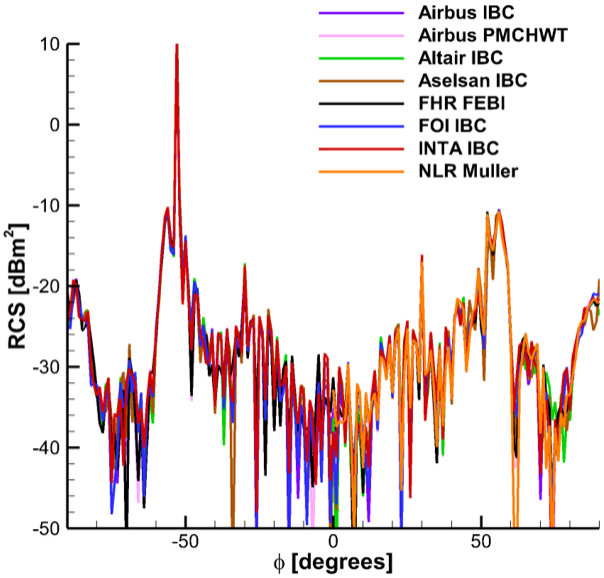

(b)

Fig. 11. Comparison of simulations of the treated model at zero elevation. RCS in dB m^2: (a) horizontal polarization and (b) vertical polarization.

edge reduces the RCS by 20 dB around $\phi = 53^o$. Also, and more importantly, the nose-on RCS is reduced significantly, even without treatment of the rim of the inlet. Scatter in the simulation results only occurs at low RCS levels, below -30dBm^2. It is precisely for this reason that the validation model is developed. Despite the large range of methods and meshes, the computational results compare very well even at very low RCS levels.

Figure 12 shows a close-up of the RCS in the nose-on region at higher aspect resolution of 0.2 degrees. At

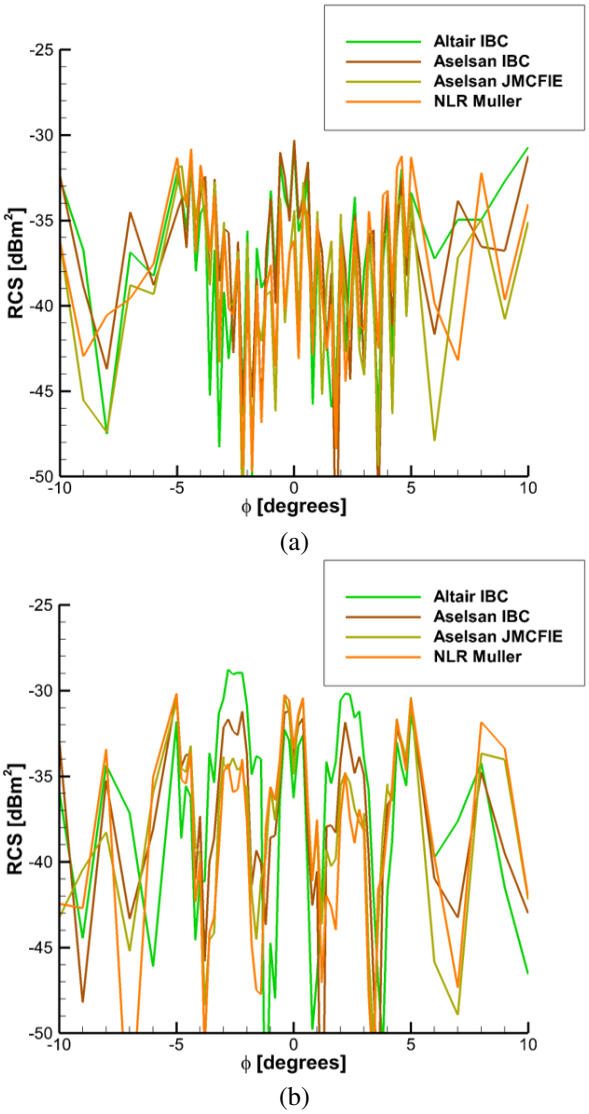

Fig. 12. Comparison of simulations of the treated model. Detail for nose-on aspects: (a) horizontal polarization and (b) vertical polarization.

these low RCS levels, differences of up to 5 dB can be observed. A more consistent cross-comparison of methods and meshes will be executed in the future.

VI. CONCLUSION

A design of a measurement model of an unmanned aerial vehicle which is geometrically complex, applies radar-absorbing material and has a low radar signature has been presented. Numerical simulations have demonstrated that the measurement model is low observable at the center frequency of 10 GHz. Experiments on a variety of cone-sphere specimens have shown that it is reasonable to expect that the surface of the measurement model can be modeled as smooth and contiguous, even though the measurement model consists of three parts and the midsection is 3D printed. Hence, it is expected that the measurement model, once built, will satisfy the design requirements.

REFERENCES

[1] A. C. Woo, H. T. G. Wang, M. J. Schuh, and M. L. Sanders, "EM programmer's notebook - benchmark plate radar targets for the validation of computational electromagnetics programs," *IEEE A&P Magazine*, vol. 34, no. 6, pp. 52-56, 1992.

[2] A. Greenwood, "Electromagnetic code consortium benchmarks," Technical Report AFRL-DE-TR-2001-1086, Air Force Research Laboratory, 2001.

[3] R. Fernandez-Recio, A. Jurado-Lucena, B. Errasti-Alcala, D. Poyatos-Martinez, D. Escot-Bocanegra, and I. Montiel-Sanchez, "RCS measurements and predictions of different targets for radar benchmark purpose," in *2009 International Conference on Electromagnetics in Advanced Applications*, Turin, Italy, 2009.

[4] J. W. Massey, J. T. Kelley, C. Courtney, D. A. Chamulak, and A. E. Yilmaz, "A benchmark suite for quantifying RCS simulation performance on modern computers," in *Proc. USNC/URSI Radio Science Meeting*, July 2018.

[5] J. T. Kelley, A. E. Yilmaz, D. A. Chamulak, and C. C. Courtney, "Increasing the material diversity in the Austin RCS benchmark suite using thin plates," in *Antenna Measurement Techniques Association Symposium (AMTA),* Newport, RI, 2020.

[6] IEEE Standard for Validation of Computational Electromagnetics Computer Modeling and Simulations, in IEEE Std 1597.1-2022 (Revision of IEEE Std 1597.1-2008), pp. 1-52, 8 Sep. 2022.

[7] R. Nangia, M. Ghoreyshi, M. P. C. van Rooij, and R. M. Cummings, "Aerodynamic design assessment and comparison of the MULDICON UCAV concept," *Aerospace Science and Tech.,* vol. 93, 2019.

[8] NATO/STO/SET-252 on *Development of a validation model of a stealth UCAV* [Online]. Available: https://www.sto.nato.int/publications/STO%20Technical%20Reports/Forms/Technical%20Report%20Document%20Set/docsethomepage.aspx?ID=5162&FolderCTID=0x0120D5200078F9E87043356C409A0D30823AFA16F6010066D541ED10A62C40B2AB0FEBE9841A61&List=92d5819c-e6ec-4241-aa4e-57bf918681b1&RootFolder=%2Fpublications%2FSTO%20Technical%20Reports%2FSTO%2DTR%2DSET%2D252

[9] A. Altinoklu, A. K. Ozturk, and M. E. Inal, "Radar cross section reduction for air vehicles based on MLFMA and surface integral equations using RAPID" in *Proceedings of ASELSAN REHIS TTEK Conference*, Ankara, Turkiye, 2021.

[10] A. Altınoklu, A. K. Ozturk, E. Sever, and M. E. İnal, "3-D scattering center determination algorithm for detecting primary radar cross-section contributing regions on a radar target," in *Proc. IEEE Int. Symp. Antennas Propag. (APSURSI),* Oregon, Portland, July 2023.

[11] E. R. Biglete, M.C.E. Manuel, J. C. Dela Cruz, M. S. Verdadero, J. M. B. Diesta, D. N. G. Miralpez, R. A. C. Javier, and J. I. C. Picato, "Surface roughness analysis of 3D printed parts using response surface modeling," in *2020 11th IEEE Control and System Graduate Research Colloquium (ICSGRC),* Shah Alam, Malaysia, pp. 191-196, 2020.

[12] R. Rakshit, A. Ghosal, P. K. S. Podder, D. Misra, and S. C. Panja, "An experimental investigation of surface roughness and print duration on FDM printed polylactic acid (PLA) parts," in *2022 Interdisciplinary Research in Technology and Management (IRTM),* Kolkata, India, pp. 1-5, 2022.

[13] Fused filament fabrication [Online]. Available: https://en.wikipedia.org/wiki/Fused_filament_fabrication

[14] Kontakt Chemie [Online]. Available: http://www.kontaktchemie.com/KOC/KOCproductdetailV2.csp?product=EMI%2035

[15] North 3D Filament [Online]. Available: https://addnorth.com/product/ESD%20PETG/ESD%20PETG%20-%201.75mm%20-%20750g%20-%20Black

[16] Altair Feko [Online]. Available: https://www.altair.com/feko

[17] Laird [Online]. Available: https://www.laird.com/products/microwave-absorbers/microwave-absorbing-elastomers-and-films/eccosorb-fgm/21191167

[18] J. Alvarez, J. M. Alonso-Rodriguez, H. Carbajosa-Cobaleda, M. R. Cabello, R. Gomez-Martin, and S. G. Garcia, "DGTD for a class of low-observable targets: A comparison with MoM and (2,2) FDTD," *IEEE Ant. and Wireless Propag. Letters*, vol. 13, pp. 241-244, 2014.

[19] P. Ylä-Oijala, M. Taskinen, and S. Järvenpää, "Surface integral equation formulations for solving electromagnetic scattering problems with iterative methods," *Radio Science*, vol. 40, no. 6, p. RS6002, 2005.

[20] A. Tzoulis and T. F. Eibert, "A hybrid FEBI-MLFMM-UTD method for numerical solutions of electromagnetic problems including arbitrarily shaped and electrically large objects," *IEEE Trans. Antennas Propag.,* vol. 53, pp. 3358-3366, Oct. 2005.

[21] H. van der Ven, C. A. Liontas, K. Cools, and D. R. van der Heul, "On the accuracy of different boundary integral formulations for dielectric bodies using RWG and BC functions," in *Proceedings of EuCAP 2016,* Davos, Switzerland, 2016.

Harmen van der Ven received his Ph.D. in Mathematics in 1993 from Utrecht University. In the same year he joined the Netherlands National Aerospace Laboratory NLR where he develops numerical algorithms for fluid dynamics and electromagnetics. His main research interest is in radar signature prediction. He is also program manager Emerging Technologies at NLR. He was the chairman of the NATO/STO group SET-252.

David Escot Bocanegra was born in Madrid, Spain. He received the M.Sc. and Ph.D. degrees in telecommunication engineering from the University of Alcala, Madrid, Spain, in 2002 and 2012, respectively. He has worked in Telecom Bretagne, Brest, France (2002-2003) and the National Institute for Aerospace Technology (INTA), Spain (2004-2019). He is since 2019 in Airbus Defence and Space, Spain. His current research interests are related to stealth technologies, radar cross section, computational electromagnetics and materials characterization.

Jesús Álvarez González was born in Leon, Spain. He received the Ph.D. degree from the University of Granada, Granada, Spain, in 2013. Since 2006, he has been working as an RCS, Antenna and EMC Engineer with Airbus Defense and Space, Getafe, Spain. His research interests include computational electrodynamics in time domain, the method of moments and fast algorithms for integral equations in frequency domain and computational electromagnetics applied to electromagnetic compatibility, antenna, and radar cross section.

Mehmet Erim İnal was born on 8 June 1971 in Mardin, Turkiye. He received the B.S. and M.S. degrees in electrical and electronics engineering from Middle East Technical University at Ankara, Turkiye, in 1993 and 1997, respectively. From 1993 till today he is employed by ASELSAN, Ankara, Turkiye. During his 30 years in the defense industry, his work mainly spans research, development and design activities of radar and electronic warfare (EW) systems, active and passive microwave devices, antennas, radomes, absorbers, frequency selective surfaces, advanced engineering materials and low observable (LO) solutions. His interest areas are interdisciplinary development cycles of critical hardware related to electromagnetics, RF and microwaves, mechanical engineering and material science. He holds several patents on antennas, absorbers and computational electromagnetics. Currently he is working as the head of "Radomes, Low Observables and Advanced Engineering Materials Design Division" in Aselsan, Ankara, Turkey.

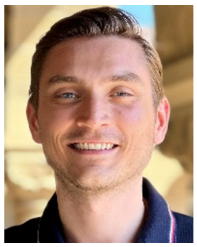

Askin Altinoklu received his B.Sc. and M.Sc. degrees in Electrical and Electronics Engineering from Middle East Technical University, Turkey, in 2016 and 2019, respectively. From July 2016 to November 2023, he worked as an RF/Microwave design engineer at ASELSAN, Turkey, where he served as a team leader for the electromagnetic analysis team from 2019 to 2023. Currently, he is a Doctoral Research Fellow in the School of Computer Science and Electronic Engineering at the University of Essex, UK, where he is involved in the research and development activities in the SCION project funded by the European Commission within the Horizon Europe, Marie Skłodowska-Curie Actions – Doctoral Network Program. His research interests lie in machine-type communications, 6G, Energy Harvesting and SWIPT, and Semantic Communications.

Alper Kürşat Öztürk was born in Yozgat, Turkey. He earned his B.S. and M.S. degrees in electrical and electronics engineering at Bilkent University, Ankara, Turkey, in 2000 and 2002, respectively. He later earned his Ph.D. from Concordia University, Montreal, QC, Canada, in 2009. From 2010 to 2019, he was employed at ASELSAN, Turkey. In 2019, he founded RAPIDEM LLC, Turkey, with a focus on developing electromagnetic simulation software for RCS prediction, scattering, and antenna design. His research interests cover a broad spectrum of applied computational electromagnetics, particularly concerning integral, differential and variational equations.

Ulrich Jakobus graduated in electrical engineering from the University of Stuttgart, Germany, in 1991. He completed his Ph.D. and Habilitation and became Privatdozent at the same university in 1994 and 1997, respectively. His areas of research included numerical techniques in electromagnetics and their hybridization, antennas, EMC and bio-electromagnetics, laying the foundations for the electromagnetics simulation code Feko in 1991. Since 1998, Ulrich has been focusing on the development and commercialization of Feko. Through an acquisition, he joined Altair in 2014, where he currently oversees the development of all electromagnetic and electronic software solutions. He is a member of URSI commission B, the German VDE/ITG, Fellow of IEEE, and Fellow of ACES.

Andrey Osipov received the degrees of Diploma Physicist (with honors), Candidate of Sciences (Ph.D.), and Doctor of Sciences (Habilitation), all in physics of electromagnetic waves, from the St. Petersburg State University, St. Petersburg, Russia, in 1983, 1987 and 1996, respectively. Since 1998 he has been with the Microwaves and Radar Institute of the German Aerospace Center (DLR). His current research interests include radar cross section engineering, theory of electromagnetic scattering by canonical objects, development of high-frequency simulation tools in radar-based remote sensing and applications of metamaterials in defense and security. Dr. Osipov is the author and co-author of two monographs, more than 160 journal and conference papers and two patents.

Øystein Lie-Svendsen received his dr.scient. (Ph.D.) in physics from the University of Oslo, Norway, in 1988. From 1990-1993 he was employed as research associate at the University of Alaska, Fairbanks, working on numerical models of plasma transport in the Earth's ionosphere. From 1993 onwards he has worked at the Norwegian Defence Research Establishment (FFI), currently as principal scientist. His research topics have been space physics, continuing his work on modelling plasma transport in the solar atmosphere and the solar wind, and, more lately, radar.

Frank Weinmann received the Dr.-Ing. degree in electrical engineering from the University of Karlsruhe, Germany, in 2004. Since 2004 he is with the Fraunhofer FHR Research Institute for High Frequency Physics and Radar Techniques in Wachtberg, Germany, as a Research Engineer. In 2009, he became Teamleader of the Electromagnetic Modelling Group, in 2017 he became head of the department Antenna Technology and Electromagnetic Modelling, and since 2023 he is head of the department Antennas & Frontend. Dr. Weinmann's major areas of interest include all aspects of antenna development, metamaterials and metasurfaces, as well as propagation modeling of electromagnetic waves, high-frequency asymptotic techniques, modeling of radar signatures, and studies in the fields of wind turbine scattering as well as automotive radar.

Åsa Andersson received the M.Sc. degree in Applied Physics and Electrical Engineering and the Ph.D. degree in Theoretical Physics from Linköping University, Linköping, Sweden in 1996 and 2002, respectively. Since 2003, she has been with the Swedish Defence Research Agency (FOI), Linköping, Sweden, working with electronic warfare modeling, advanced low observable materials and radar signatures. Her present activities are focused on research and applications of electromagnetic modeling and calculations of radar signatures for military systems.

Henrik Edefur graduated from the Royal Institute of Technology (KTH) in Stockholm 2002 with a master degree in aeronautics. He started working at FOI 2004 as a research engineer and was last year appointed to senior scientist. All this time at FOI he has been working with aircraft conceptual design and analysis.

Jan-Ove Hall obtained his M.Sc. in 2000 and a Ph.D. in space physics in 2004, both from Uppsala University in Sweden. Subsequent to completing his doctoral studies, Dr. Hall embarked on a postdoctoral research position. In 2006, he transitioned to the Swedish Defence Research Agency (FOI), where he conducts research in radar signature management.

David Poyatos received his M.Sc. degree in Telecommunication Engineering from the Universidad Politécnica de Madrid (UPM), Spain, in 1998 and a Ph.D. degree in Computational and Applied Electromagnetics from the University of Alcala, Spain, in 2017. He joined the National Institute of Aerospace Technology (INTA), Spain, in 1997. Since 2015, he is the head of the Radiofrequency Area at INTA. His current research activities are related to the simulation, measurement and analysis of antennas and radar signature and the electromagnetic characterization of materials.

Tolga Çiftçi received the B.Sc. degree in Electrical and Electronics Engineering from Bilkent University, Ankara, Turkey, in 2012, and the M.Sc. degree in Industrial Engineering from Middle East Technical University, Ankara, Turkey in 2019. Since 2016, he has been with Turkish Aerospace Industries, currently working as Lead Engineer. His current research interests include computational electromagnetics, optimization techniques, electromagnetic analysis, electromagnetic compatibility and electromagnetic testing.

Şükrü Tarık Kostak received the B.Sc. degree in Mechanical Engineering from Istanbul Technical University (ITU), Istanbul, Turkey, in 2018. Since 2018, he has been with Turkish Aerospace Industries, currently working as Structural Design Chief Engineer. His current research interest is development of next generation fighter aircrafts.